Prediction of iron(II) breakthrough in adsorptive filters under anoxic conditions

Saroj K. Sharma, Branislav Petrusevski, Bas Heijman and Jan C. Schippers

ABSTRACT

Physical, chemical and biological mechanisms may contribute to the removal of iron in filters. This paper focuses on the physical–chemical mechanisms namely adsorptive filtration and floc filtration. Iron removal filters operating in physical–chemical mode are expected to perform better in terms of filtrate quality, run time and costs by changing the governing mode of operation from floc filtration to adsorptive filtration. In adsorptive filtration, iron(II) ions adsorb onto iron oxide coating on the filter media and are subsequently oxidised to iron(III). Modelling of adsorptive iron removal is an essential tool to predict the performance of filters operated under adsorptive mode and to optimise design parameters for adsorptive iron removal filters. The iron concentration in filtrates of adsorptive filters with new (fresh, uncoated) and iron oxide coated sand operating under anoxic conditions, was modelled using adsorption isotherm, mass balance and mass transfer equations. Kinetic rate constants, isotherm parameters and mass transfer coefficients used for model predictions were determined from batch and short column experiments. The measured filtrate iron concentrations of laboratory filter columns were then compared with the predictions of three different fixed bed adsorption models. Consideration of external mass transfer alone (constant pattern model, CPM) was not sufficient to predict the increase of filtrate iron concentration with time. Further improvement in prediction was observed when the linear driving force model (LDFM) was used and the effect of dispersion was also included in the model. The inclusion of surface diffusion (plug flow homogeneous surface diffusion model, PFHSDM) improved model predictions significantly compared with the CPM. The LDFM and the PFHSDM predictions of iron breakthrough were better in the case of new sand compared with iron oxide coated sand. The difference in model predictions and experimental results in the case of coated sand was probably due to initial pH drop in the pores of the filter media with iron(II) adsorption, and a consequent decrease in iron(II) adsorption capacity.

Key words | adsorptive filtration, breakthrough, groundwater, iron removal, modelling, prediction

Saroj K. Sharma (corresponding author)
Branislav Petrusevski
Jan C. Schippers
International Institute for Infrastructural, Hydraulic and Environmental Engineering (IHE),
PO Box 3015,
2601 DA,
Delft,
The Netherlands
E-mail: *roj@ihe.nl*

Bas Heijman
Jan C. Schippers
Kiwa NV Water Research,
PO Box 1072,
3430 BB,
Nieuwegein,
The Netherlands

INTRODUCTION

Conventionally, iron is removed from groundwater by the processes of aeration and rapid filtration (O'Connor 1971; Salvato 1992). Different mechanisms (physical, chemical and biological) may contribute to iron removal in filters but the dominant one depends on the physical and chemical characteristics of the water and process conditions applied (Rott 1985; Hatva 1989; Mouchet 1992; Søgaard *et al.* 2000). Oxidation-floc formation (floc filtration) and adsorption-oxidation (adsorptive filtration) are the two main physicochemical mechanisms of iron removal in filters. This paper focuses mainly on adsorptive filtration mechanism of iron removal.

In floc filtration, soluble iron(II) present in groundwater is oxidised to insoluble iron(III) and the flocs formed are removed in filters. In adsorptive filtration, the iron(II) present in anoxic groundwater is removed by adsorption onto the surface of the filter media. The adsorbed iron(II) is oxidised in the presence of oxygen

thus creating a new surface for adsorption and consequently allowing the continuation of the process. Under commonly applied treatment conditions, the floc filtration mode is commonly believed to predominate. The adsorptive filtration mode of iron removal, however, has several advantages over the floc filtration mode, namely: longer filter run, shorter filter ripening time, and less backwash water use and sludge production (Sharma *et al.* 2001).

Adsorption of iron(II) onto iron hydroxide flocs and iron oxide coated sand is well known (O'Connor 1971; Tamura *et al.* 1976). Adsorption is also the main mechanism of subsurface iron removal (Braester & Martinell 1988; Appelo *et al.* 1999). Iron oxide coated filter media from iron removal plants has a high iron(II) adsorption capacity (Sharma *et al.* 1999) which can be utilised to improve iron removal in filters. There are strong indications that many plants with iron oxide coated sand will perform better in terms of filtrate quality and costs when the mode of operation is switched from predominantly floc filtration to predominantly adsorptive filtration (Sharma *et al.* 1999, 2001, 2002).

A model describing adsorptive iron removal in filters could be an essential tool to predict the performance of existing filters when operated in adsorptive mode. Such a model could also be used to evaluate the effects of various process and operational variables on process efficiency and, consequently, to help to establish optimal design parameters for iron removal filters operating in adsorptive mode. Additionally, prediction of the breakthrough with a mathematical model can reduce the need for lengthy and costly pilot experiments.

To achieve principally adsorptive iron removal, the filters can be operated in two modes: intermittent regeneration mode and continuous regeneration mode. This paper deals with the modelling and prediction of iron(II) breakthrough in filtration columns with new and iron oxide coated sand under anoxic conditions (intermittent regeneration mode). It should be noted that, in the absence of oxygen, other mechanisms of iron removal, namely, oxidation-floc filtration and biological oxidation will not take place and hence adsorptive iron removal is the only removal mechanism possible.

THEORETICAL BACKGROUND

Reaction mechanism

Adsorption of iron(II) onto the surface of filter media can be represented by (Takai 1973; Barry *et al.* 1994):

$$\equiv S\text{-}OH + Fe^{2+} \rightleftarrows \equiv S\text{-}OFe^{+} + H^{+} \tag{1}$$

where ≡S represents the surface of the filter media.

In the presence of oxygen, the adsorbed iron(II) is oxidised creating a new surface.

$$\equiv S\text{-}OFe^{+} + \frac{1}{4}O_2 + \frac{3}{2}H_2O \rightarrow \equiv S\text{-}OFe\left\langle \begin{matrix} OH \\ OH \end{matrix} + H^{+} \right. \tag{2}$$

From Equations (1) and (2)

$$\equiv S\text{-}OH + Fe^{2+} + \frac{1}{4}O_2 + \frac{3}{2}H_2O \rightarrow \equiv S\text{-}OFe\left\langle \begin{matrix} OH \\ OH \end{matrix} + 2H^{+} \right. \tag{3}$$

Thus, the adsorption sites are regenerated and hence the process continues.

Prediction of breakthrough

Two main steps are required before adsorbates can be attached to the adsorbent surface: (i) transport of iron(II) from the bulk solution to the adsorbent surface, and (ii) adsorption of the iron(II) on the adsorbent sites. Adsorption reactions are generally very fast (Ruthven 1984; Tien 1994), therefore the mechanism of adsorption of iron(II) onto the surface of the filter media is assumed to be mass transfer controlled.

The mass balances for an isothermal plug flow system with dispersion, consisting of spherical particles, can be written as (Ruthven 1984; Faust & Aly 1987; Tien 1994):

$$v_i\frac{\partial c}{\partial z} + \rho\frac{(1-\varepsilon)}{\varepsilon}\frac{\partial q}{\partial t} + \frac{\partial c}{\partial t} - D_L\frac{\partial^2 c}{\partial z^2} = 0 \tag{4}$$

$$\frac{\partial q}{\partial t} = D_s\left(\frac{\partial^2 q}{\partial r^2} + \frac{2\partial q}{r\partial r}\right) \tag{5}$$

Adsorption isotherm:

$$q_s = f(c_s) \tag{6}$$

The initial and boundary conditions are

$$c = c_0 + \left(\frac{D_L}{v_i}\right)\frac{\partial c}{\partial z} \quad \text{at} \quad z = 0 \tag{7}$$

$$\frac{\partial c}{\partial z} = 0 \quad \text{at} \quad z = L \tag{8}$$

$$\frac{\partial q}{\partial r} = 0 \quad \text{at} \quad r = 0 \tag{9}$$

$$\frac{\partial q}{\partial r} = \frac{k_f}{D_{s\rho}}(\text{c-c}_s) \quad at\ r = R \tag{10}$$

$$c = 0 \text{ at } t = 0 \tag{11}$$

$$q = 0 \text{ at } t = 0 \tag{12}$$

where,

q = solid phase iron(II) concentration (kg kg^{-1})
D_L = dispersion coefficient (m^2 sec^{-1})
q_s = solid phase iron(II) concentration in equilibrium with c_s (kg kg^{-1})
D_s = effective surface diffusivity (m^2 sec^{-1})
r = radial distance in particle (m)
z = longitudinal distance in the column (m)
t = time (s)
c = liquid phase iron(II) concentration (kg m^{-3})
c_s = liquid phase iron(II) concentration near the particle surface (kg m^{-3})
c_0 = influent iron(II) concentration (kg m^{-3})
v_i = interstitial liquid velocity (m sec^{-1})
k_f = external mass transfer coefficient (m sec^{-1})
R = radius of the filter bed particles (m)
ε = fixed bed porosity (dimensionless)
ρ = particle density (kg m^{-3})
L = length of the column (m)

Several analytical and numerical solutions of these equations are available for the prediction of breakthrough in fixed bed adsorbers (Ruthven 1984; Sontheimer *et al.* 1988; Smith 1991; Tien 1994). The prediction of iron breakthrough requires an accurate determination of isotherm parameters and mass transfer coefficients. In this study, the iron(II) breakthrough in the adsorptive filter was predicted by solving the above set of equations using three different models with increasing complexity, namely: constant pattern model, linear driving force model and plug flow homogeneous surface diffusion model. The predicted values were then compared with the results of laboratory-scale filter column experiments.

Constant pattern model

As the first simplification, it was hypothesised that the internal surface area of the filter media plays a minor role in the adsorptive iron removal process and there is no axial dispersion in the filtration columns ($D_L = 0$). Hence, the influence of internal mass transfer and axial dispersion on iron(II) adsorption was neglected. For this case, the iron(II) breakthrough was predicted using the constant pattern solution of an isothermal plug flow system with a linear-rate liquid-film mass transfer resistance model for Langmuir equilibrium given by Michaels (1952) for fixed bed ion exchange (Ruthven 1984; Wankat 1990). For this case the rate equation (5) can be replaced by:

$$\frac{\partial q}{\partial t} = k'(c - c_s = \frac{3k_f}{R\rho(1-\epsilon)}(c - c_s) \tag{5a}$$

where k' is the adsorption rate constant.

The Langmuir adsorption isotherm is given by:

$$q_s = \frac{bq_m c_s}{1 + bc_s} \tag{6a}$$

where b (m^3 kg^{-1}) and q_m (kg kg^{-1}) are Langmuir isotherm constants.

The shape of the breakthrough curve is given by equations (13) and (14)

$$\frac{k'c_o}{q_0}(t_2 - t_1) = \frac{1}{\lambda} ln\left(\frac{\phi_2(1-\phi_1)}{\phi_1(1-\phi_2)}\right) + ln\left(\frac{1-\phi_2}{1-\phi_1}\right) \tag{13}$$

$$k' = \frac{3k_f}{R\rho(1-\varepsilon)},\ \phi_1 = \frac{c_1}{c_o},\ \phi_2 = \frac{c_2}{c_o}, \lambda = 1-\beta,\ \beta = 1-\frac{q_0}{q_m} \qquad (14)$$

where q_0 = solid phase concentration in equilibrium with c_0.

The external mass transfer coefficient k_f is related to the Sherwood number Sh via the equation

$$k_f = \frac{\mathrm{Sh}.D_{AB}}{2R} \qquad (15)$$

where D_{AB} is the diffusion coefficient of iron(II) in water ($m^2\ sec^{-1}$).

The Sherwood number Sh was computed using the mass transfer correlation given by Wilson and Geankoplis (1966) for fixed beds of spherical particles with bed porosity between 0.35 and 0.75 given by:

$$\mathrm{Sh} = \frac{1.09}{\varepsilon}\mathrm{Re}^{1/3}\mathrm{Sc}^{1/3} \quad \text{for} \quad 0.0016<\mathrm{Re}<55$$
$$\text{and } 165<\mathrm{Sc}<70600 \qquad (16)$$

where Re and Sc are the Reynolds number and Schmidt number, respectively, given by the following equations:

$$\mathrm{Re} = \frac{2Rv_0}{\nu} \quad \mathrm{Sc} = \frac{\nu}{\mathrm{D_{AB}}} \qquad (17)$$

where v_0 = average superficial velocity ($m\ sec^{-1}$) and ν = kinematic viscosity ($m^2\ sec^{-1}$).

Linear driving force model

The linear driving force (LDF) model is a simplified approach that uses an overall kinetic rate constant (covering both internal and external mass transfer coefficients) for the adsorption rate equation. It is postulated that the uptake rate of adsorbate by an adsorbent is linearly proportional to the driving force, defined as the difference between the surface concentration and the average adsorbed phase concentration (Peel & Benedek 1981; Tien 1994). Mathematically, the solid phase mass balance is given by the linear driving force equation:

$$\frac{\partial q}{\partial t} = k(q_s - q) \qquad (5b)$$

where k is LDF kinetic rate constant (sec^{-1}).

Using mass balance and the Freundlich isotherm equation, the LDF equation for a batch system can be transformed in terms of concentration as

$$c = (c_0 - c_s)e^{-kt} + c_s \qquad (18)$$

In logarithmic form,

$$ln\left(\frac{c-c_s}{c_0-c_s}\right) = -kt$$

The LDF rate constant k can, therefore, be obtained from the kinetic data of batch adsorption experiments (Heijman *et al.* 1999).

In this case, the axial dispersion in the filtration column was also included and the Freundlich isotherm equation was used for equilibrium. The Freundlich isotherm equation is given by:

$$q_s = Kc_s^n \qquad (6b)$$

where K and n are constants for the Freundlich isotherm. These constants are determined from the adsorption equilibrium experiments.

The model equations (4) to (12) were solved numerically using the PDESOL software to obtain the iron(II) breakthrough curves.

Plug flow homogeneous surface diffusion model

The plug flow homogeneous surface diffusion model (PFHSDM), developed for modelling adsorption in activated carbon, uses Freundlich isotherm parameters K and n and mass transfer coefficients k_f and D_s for the prediction of the breakthrough (Liu & Weber 1981; Hand *et al.* 1983; Sontheimer *et al.* 1988). The PFHSDM considers the dual mass transfer mechanism of film diffusion across the hydrodynamic boundary layer of the solid and intraparticle resistance in the form of surface diffusion. The mass transfer coefficients are determined by fitting the

Table 1 | Characteristics of the new and iron oxide coated sand used

Media	New sand	Coated sand
Grain size (mm)	0.8–1.25	0.7–1.25
Mean diameter (mm)	0.82	0.81
Average geometric surface area ($m^2\ g^{-1}$)	2.8×10^{-3}	2.8×10^{-3}
Specific surface area (BET) ($m^2\ g^{-1}$)	1.0	11.4
Surface extractable iron content (mg g^{-1} sand)	0	29–33
Pore volume ($cm^3\ g^{-1}$)		
Micropore volume (diameter <2 nm)	0.06×10^{-3}	4.9×10^{-3}
Mesopore volume (2 nm $<$ diameter $<$ 50 nm)	1.24×10^{-3}	6.7×10^{-3}
Total pore volume ($cm^3\ g^{-1}$)	1.30×10^{-3}	11.6×10^{-3}
Time in use (years)	—	3.5
Process conditions during coating development	—	Filtration rate ~8 m h^{-1}; pH = 7.6, Fe = 1.7 mg l^{-1} Mn = 0.07 mg l^{-1}, HCO_3^- = 155 mg l^{-1}

PFHSDM to the breakthrough of the target substance in short column tests (Weber & Liu 1980).

In this case, the axial dispersion in the filtration columns was not considered and the model equations (4) to (12) were solved numerically using the computer program written by Yuasa (1982).

MATERIALS AND METHODS

Filter media

New (virgin, uncoated) sand and iron oxide coated sand from a full-scale groundwater treatment plant in the Netherlands were used in this study. The characteristics of the filter media used are presented in Table 1. The specific surface areas and pore volumes were measured using the BET nitrogen gas adsorption method with a Quantachrome Autosorb-6B gas adsorption analyser at 77 K. The new sand was washed in demineralised water, soaked in concentrated HCl (pH$<$2) for 24 h and again rinsed with demineralised water and dried at 40°C. The iron oxide coated sand was washed gently with demineralised water to remove any deposits and dried at room temperature before using for batch and column experiments.

Batch experiments

Batch adsorption experiments were conducted to obtain isotherm parameters and LDF kinetic rate constants. Iron(II) adsorption onto new and iron oxide coated sand was measured at different pH by conducting experiments at room temperature (18–20°C). The experimental set-up and procedure to determine iron(II) adsorption onto the filter media was similar to that used in an earlier study (Sharma *et al.* 1999). Nitrogen gas was used for deoxygenation and the pH was adjusted using HCO_3^--CO_2 buffer. Different amounts of $FeSO_4 \cdot 7H_2O$ stock solution

were introduced into the closed reactor containing deoxygenated water and a known weight of filter media. Samples were taken periodically from the reactor until equilibrium iron concentration was reached and the iron concentrations were measured (Standard Methods 1995). Iron(II) adsorbed onto the media as a function of time was calculated from the iron mass balance. Adsorption isotherm constants were obtained by fitting isotherm models (Equations 6a and 6b) to iron(II) adsorbed onto filter media at various equilibrium iron concentrations.

The LDF rate constants (k) for both filter media at different pH were calculated by fitting Equation (19) to kinetic (time versus iron concentration) data of the batch adsorption experiments. The constant k is given by the slope of the straight line when $\ln(c - c_s)/(c_0 - c_s)$ is plotted against time.

Column experiments

Laboratory-scale column experiments were conducted using a 25 mm ID, 55 cm high plexiglass column to obtain iron(II) breakthrough profiles. The depth of the filter media was 50 cm. Nitrogen gas was used to prepare the anoxic feed water. Model (artificial) groundwater used in the experiments was prepared by mixing $FeSO_4 \cdot 7H_2O$ stock solution in deoxygenated demineralised water buffered with $NaHCO_3$ to achieve an initial iron(II) concentration of 4 mg l^{-1} and an alkalinity of 100 mg l^{-1} of HCO_3^-. The pH was adjusted with HCl and NaOH. The column experiments were conducted at three different pH values i.e. 6.0, 6.5 and 7.0. The filtration rate was 8 m h^{-1} for new sand and 4 m h^{-1} for coated sand. The pH and oxygen concentration of the feed water were monitored continuously to ensure constant pH and anoxic conditions.

Before starting the filter run, the columns were brought to equilibration by recirculating the demineralised water adjusted to the pH and alkalinity of the subsequent run through the columns for about 15 min. The feed water and filtrate iron concentrations were measured periodically during the filter run to obtain the relative iron concentration (c/c_0) breakthrough profiles. In the case of coated sand, column experiments were terminated after a run time of 10 h.

Table 2 | Process conditions for short column experiments

Media	Bed depth (cm)	Superficial velocity (m h^{-1})
New sand	7	8
Coated sand	4	4

Determination of dispersion coefficients

The conductivity (NaCl) breakthrough experiments (without iron(II)) were conducted separately for the 50 cm-long columns equipped with new and iron oxide coated sand to assess the extent of axial dispersion in the packed bed. Concentrated sodium chloride solution (1 g NaCl l^{-1}) was introduced into the column containing filter media and the conductivities of the samples taken periodically were measured until complete breakthrough. Axial dispersion coefficients D_L were then determined by solving the model Equations (4) to (12) numerically using the PDESOL software, after equating the adsorption term ($\partial q/\partial t$) to zero. The axial dispersion coefficients obtained in this way were used to predict the iron(II) breakthrough in the adsorptive filter columns with the LDFM.

Determination of mass transfer coefficients

Short column experiments were conducted separately for both media at pH 6.5 using the same model groundwater to obtain the external mass transfer coefficient (k_f) and surface diffusion coefficient (D_s). The bed depths of the short columns were selected after conducting several trial experiments in order to get the complete breakthrough curve within a short time. The operational parameters for short column tests are summarised in Table 2.

The mass transfer coefficients k_f and D_s were obtained by fitting the PFHSDM to the iron breakthrough data of short column experiments using the computer program written by Yuasa (1982). These coefficients were later used for the prediction of breakthrough in long columns.

Table 3 | Adsorption isotherm parameters

			pH		
Media	**Isotherm**	**Parameter**	**6.0**	**6.5**	**7.0**
New sand	Freundlich	K	6.4×10^{-6}	6.9×10^{-6}	1.1×10^{-5}
		n	0.54	0.73	0.70
		r^2	0.95	0.98	0.98
	Langmuir	q_m	3.1×10^{-5}	6.2×10^{-5}	6.3×10^{-5}
		b	0.22	0.115	0.208
		r^2	0.97	0.98	0.96
Coated sand	Freundlich	K	1.2×10^{-4}	1.7×10^{-4}	3.3×10^{-4}
		n	0.49	0.54	0.43
		r^2	0.96	0.99	0.98
	Langmuir	q_m	4.1×10^{-4}	7.5×10^{-4}	9.2×10^{-4}
		b	0.374	0.26	0.514
		r^2	0.94	0.98	0.93

Units: K [$(g\ g^{-1})/(g\ m^{-3})^n$], n [–], q_m [$g\ g^{-1}$], and b [$m^3\ g^{-1}$].

RESULTS AND DISCUSSION

Isotherm parameters

Adsorption isotherm constants obtained by fitting Freundlich and Langmuir isotherm models to batch equilibrium experimental results are presented in Table 3. Batch results showed that adsorption of iron(II) onto both new and iron oxide coated sand gave 'favourable' adsorption isotherms ($n<1$). Systems with favourable adsorption isotherms show 'constant pattern' behaviour with respect to the form of mass transfer front or removal profiles along the depth of the filter, i.e. the breakthrough curve retains a constant shape (Ruthven 1984; Wankat 1990; Tien 1994). Therefore, the constant pattern model was the first to be selected for the prediction of iron breakthrough in adsorptive filter columns.

Model predictions

Constant pattern model

In the constant pattern model (CPM), internal mass transfer and axial dispersion in the column were neglected. The film mass transfer coefficients (k_f) for the new and iron oxide coated sand were computed from Equations (15) to (17). Using the viscosity of water of $10^{-6}\ m^2\ sec^{-1}$ (at 20°C) and diffusion coefficient of iron(II) as $0.72 \times 10^{-9}\ m^2\ sec^{-1}$ (CRC Handbook 1996), the external mass transfer coefficient k_f for new and iron oxide coated sand was calculated to be 3.26×10^{-5} m sec^{-1} and 2.61×10^{-5} m sec^{-1}, respectively.

Figures 1 and 2 compare the iron breakthrough curves predicted from Equations (13) to (17) and the experimental data at different pH values for the filter columns with

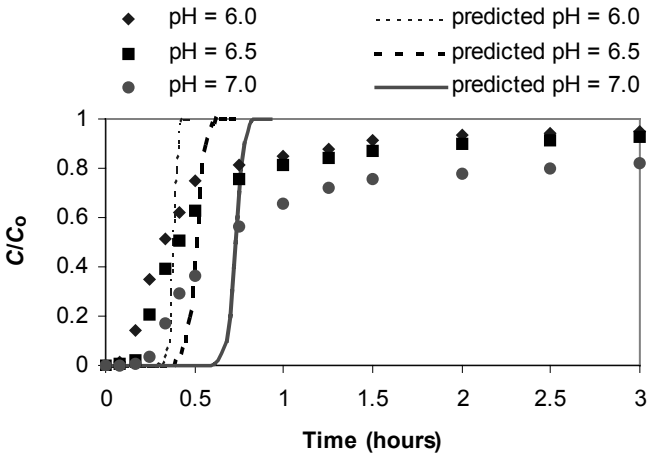

Figure 1 | Predicted (CPM) and experimental iron breakthrough curves for the filter column with new sand at different pH (filtration rate=8 m h^{-1}, initial iron concentration=4 mg l^{-1}).

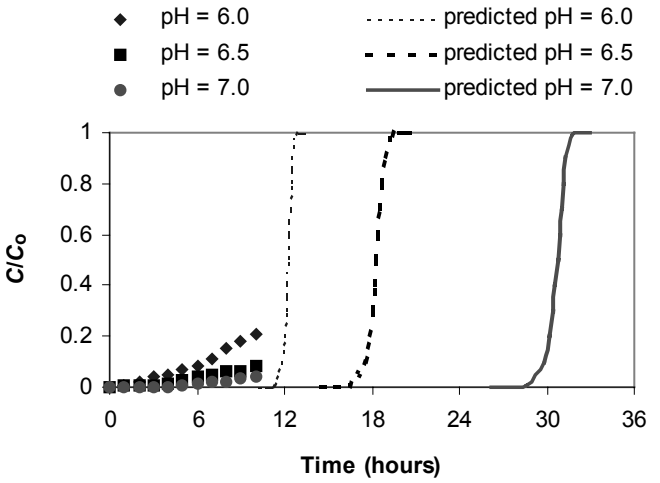

Figure 2 | Predicted (CPM) and experimental iron breakthrough curves for the filter column with iron oxide coated sand at different pH (filtration rate=4 m h^{-1}, initial iron concentration=4 mg l^{-1}).

new and iron oxide coated sand, respectively. It was observed that (i) the iron breakthrough in the experimental columns occurred much earlier than predicted by the model, and (ii) at the later stage, the increase of filtrate iron concentrations in experimental columns was considerably slower while the model predicted a sharp increase in iron concentration. This indicates that the overall mass transfers in adsorptive iron removal filters are likely to be much slower than that predicted by the CPM. In

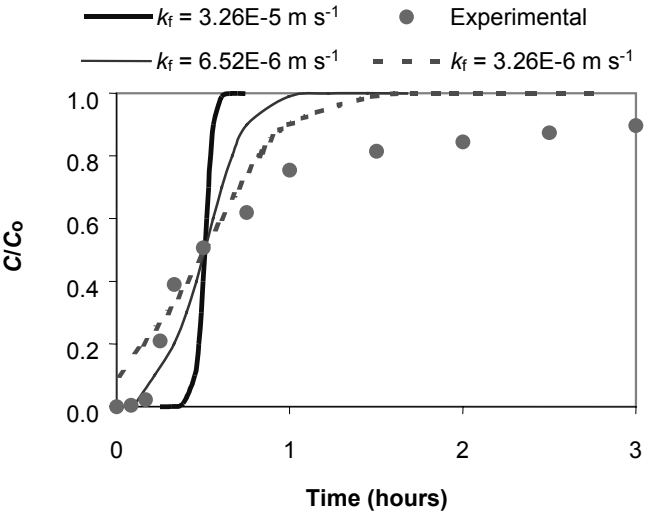

Figure 3 | Experimental and predicted iron breakthrough curves for the filter column with new sand for different values of external mass transfer coefficient k_f (filtration rate=8 m h^{-1}, initial iron concentration=4 mg l^{-1}, pH=6.5).

particular, the internal mass transfer is most likely a limiting factor, as this is not taken into account in the CPM.

Figure 3 shows that even when external mass transfer coefficient k_f is decreased by 5 or 10 times, there are still considerable differences between model predictions and experimental data. This implies that, besides external mass transfer, there are also some other factors that affect the adsorptive iron removal process. The iron(II) breakthrough might be influenced by adsorption of iron(II) onto the internal surfaces, or the internal mass transfer might play a role in the removal process. Therefore, the consideration of external film mass transfer alone was not sufficient to model accurately the process of adsorptive iron removal.

Linear driving force model

As the CPM was not satisfactory, the LDFM including the axial dispersion in the columns was applied to get better predictions of iron breakthrough in adsorptive columns. The LDF overall kinetic rate constant (k) was obtained by fitting Equation (19) to kinetic data (iron concentration versus time) of batch adsorption experiments. The LDF

Table 4 | LDF rate constants at different pH

Media	LDF rate constant k (s^{-1})		
pH	6.0	6.5	7.0
New sand	2.6×10^{-4}	2.8×10^{-4}	2.9×10^{-4}
Coated sand	1.7×10^{-4}	1.8×10^{-4}	2.0×10^{-4}

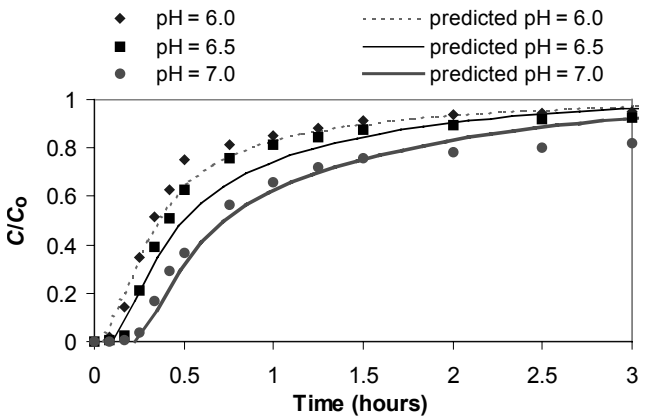

Figure 4 | Predicted (LDFM) and experimental iron breakthrough curves for the filter column with new sand (filtration rate=8 m h^{-1}, initial iron concentration=4 mg l^{-1}).

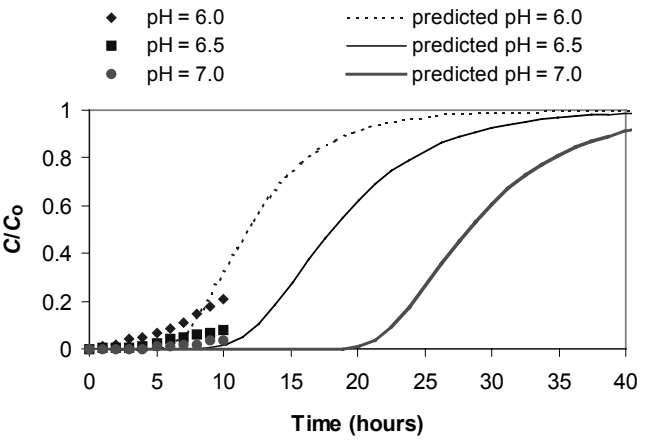

Figure 5 | Predicted (LDFM) and experimental iron breakthrough curves for the filter column with iron oxide coated sand (filtration rate=4 m h^{-1}, initial iron concentration=4 mg l^{-1}).

kinetic rate constants for new and coated sand at different pH are summarised in Table 4.

Axial dispersions in the experimental columns were measured by performing the conductivity (NaCl) breakthrough experiments. Using the model Equations (4) to (12) for the system without adsorption, the dispersion coefficients for new sand and iron oxide coated sand, under given process conditions, were determined to be $1.6 \pm 0.1 \times 10^{-4}$ m^2 sec^{-1} and $2.0 \pm 0.1 \times 10^{-4}$ m^2 sec^{-1}, respectively.

Figures 4 and 5 compare the LDFM predictions (including axial dispersion) with the experimental iron breakthrough data. Figure 4 shows that the LDFM reasonably predicted the iron(II) breakthrough in the adsorptive column with new sand. The LDFM predictions for all three pH values were very close to the experimental results. In the case of coated sand (Figure 5), the LDFM predictions of iron breakthrough were closer to the experimental data than that of the CPM. However, there was still a considerable difference between the experimental data and the LDFM predictions in the case of coated sand.

The dispersion in a fixed bed adsorber depends on the column geometry and the flow conditions. The dispersion number (D_L/v_iL) is the measure of the degree of variation from the ideal plug flow condition (0 for plug flow and infinity for completely mixed) (Levenspiel 1972; Weber 1972). Under the applied conditions, the dispersion numbers were calculated as 0.06 and 0.14 for the experiments with new and coated sand, respectively. The effect of dispersion is likely to be more pronounced at the lower velocity and for the short columns. At higher velocity and for longer columns, the effect of dispersion is likely to be negligible (Weber 1972; Bhattarai & Griffin 1999). It is consequently likely that some dispersion effect was observed because a relatively short (50 cm) experimental column was used in this study. In practice, filter bed depth and filtration rate range between 1.5 and 2.0 m and between 5 and 15 m h^{-1}, respectively. Therefore, the dispersion effect is likely to be rather small in full-scale filters.

Plug flow homogeneous surface diffusion model

Since both models, the CPM and the LDFM, do not take into account internal and external mass transfer, the

Table 5 | Mass transfer coefficients from short column tests

Media	k_f (m s^{-1})	D_s (m^2 s^{-1})
New sand	$2.27 \pm 0.20 \times 10^{-5}$	$2.30 \pm 0.20 \times 10^{-11}$
Coated sand	$1.65 \pm 0.13 \times 10^{-5}$	$0.13 \pm 0.01 \times 10^{-11}$

PFHSDM was applied to predict iron breakthroughs in filter columns with new and iron oxide coated sand. The PFHSDM separately considers both external mass transfer and internal mass transfer. The mass transfer coefficients (k_f and D_s) obtained by fitting the PFHSDM to short column iron breakthrough data are summarised in Table 5.

The external mass transfer coefficients (k_f) for new and coated sand obtained from the short column experiments (Table 5) were 70% and 63%, respectively, of the external mass transfer coefficients calculated theoretically from mass transfer correlations. This is probably because the actual iron(II) adsorption capacity in the filter columns was smaller than the adsorption capacity obtained from the batch adsorption experiments.

Figures 6 and 7 present the iron breakthrough curves for the 50 cm column predicted from the PFHSDM (neglecting axial dispersion) together with the experimental data at different pH values for new and coated sand, respectively. Figure 6 shows that the PFHSDM fairly accurately predicted the initial increase in filtrate iron concentration in the adsorptive column with new sand. However, with the further progress of the filter run, there were considerable differences between the model predictions and experimental data. At all three pH values studied, the filtrate iron concentration did not reach the feed water iron concentration but the breakthrough curve was 'broadening'. This may be due to some continuous removal of iron in the column, which was achieved through either ion exchange or iron(II) oxidation by traces of oxygen possibly present in the pores of the filter media and in the feed water. Additionally, the sand grain is not homogeneous but consists of pores of different sizes which are narrow close to the centre of the grain.

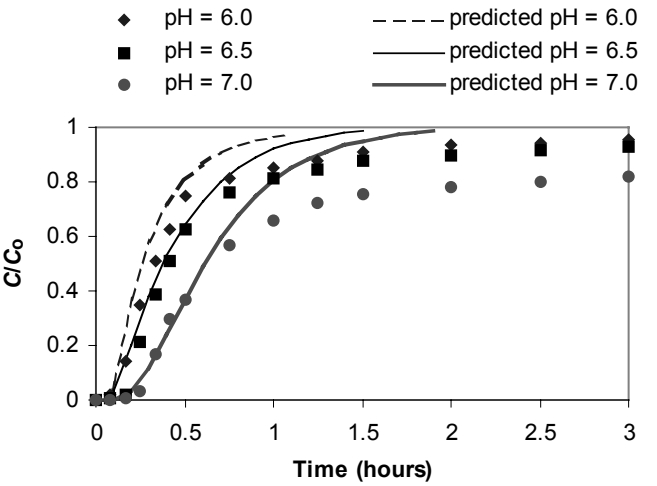

Figure 6 | Predicted (PFHSDM) and experimental iron breakthrough curves for the filter column with new sand (filtration rate=8 m h^{-1}, initial iron concentration=4 mg l^{-1}).

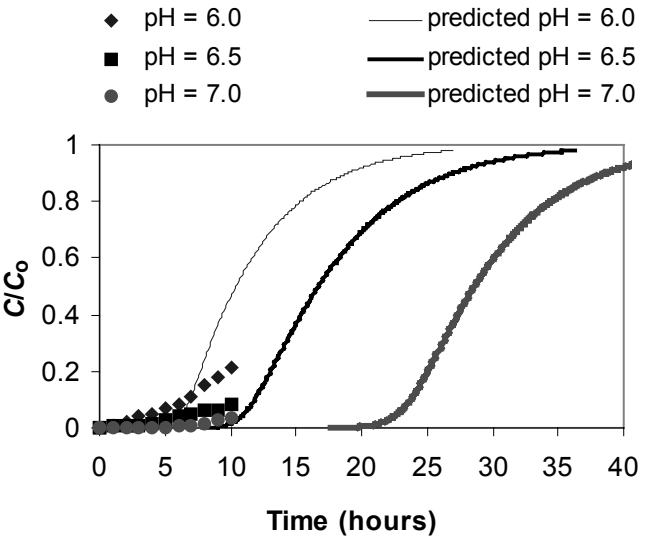

Figure 7 | Predicted (PFHSDM) and experimental iron breakthrough curves for the filter column with coated sand (filtration rate=4 m h^{-1}, initial iron concentration=4 mg l^{-1}).

Figure 7 shows that the PFHSDM provides a somewhat better prediction of the iron breakthrough in adsorptive filters with iron oxide coated sand than the CPM. However, the initial increase of iron concentration in the experimental column occurred much earlier than the model predicted. Further increase in filtrate iron concentration observed in the experiments, however, was very

slow compared with a sharp increase predicted by the model. There is not sufficient experimental data to compare the agreement of the model predictions with the later part of the breakthrough curve. For columns with iron oxide coated sand, the LDFM and the PFHSDM predictions of iron breakthrough were very similar.

The axial dispersion was not considered initially in the PFHSDM because the model considers 'plug flow' conditions and some effect of axial dispersion was already included in the mass transfer coefficients k_f and D_s determined from the short column experiments. Even when the effect of dispersion was taken into account and experimentally measured axial dispersion coefficient was included in the PFHSDM, it was found that for the measured values of k_f and D_s for new and iron oxide coated sand, there were no significant changes in the PFHDSM model predictions with or without inclusion of the axial dispersion.

The 'broadening' of the breakthrough curves in the case of new sand might be due to the presence of some traces of oxygen in the feed water (5 $\mu g\, l^{-1}$—the detection level of the oxygen meter used) which might have continuously regenerated some of the iron(II) adsorption sites, thus resulting in an extra capacity (5 $\mu g\, l^{-1}$ of oxygen can oxidise about 0.04 mg l^{-1} of iron(II)). In the case of coated sand, however, the contribution of this effect to overall removal is likely to be minimal because its iron(II) adsorption capacity is much higher than that of new sand.

It should be noted that, in the case of the short column tests, adsorption on the outer or external pore spaces probably plays a major role and determines the mass transfer coefficients. In the case of new sand, external pores are relatively larger and greater in number, so the effect of internal pores is most likely not very pronounced. However, in the case of coated sand the internal pores are likely to be considerably greater in number and relatively smaller than those in new sand. Therefore, it is likely that the actual surface diffusion coefficient D_s in the case of coated sand is much smaller than that measured from the short column tests. Hence, the actual iron breakthrough in adsorptive filters with iron oxide coated sand might be much slower than that predicted by the model.

Furthermore, the PFHSDM assumes that the adsorbent is homogeneous and the surface diffusion is the dominant mass transfer mechanism. However, the iron oxide coated sand is not homogeneous but consists of a sand core and an outer layer of iron oxide coating. Additionally, the new sand grain and the iron oxide coating are not homogeneous but consist of pores of different sizes, and the iron oxide coating is not uniform throughout the sand grain (Sharma *et al.* 2002). This is probably one of the reasons for the difference in the PFHSDM predictions and experimental results.

Sensitivity analysis of model parameters

The sensitivity of the LDFM and the PFHSDM predictions with the change in the values of model parameters (specifically adsorption capacity, mass transfer coefficients and dispersion coefficients) were analysed. This was done to check whether the differences between the experimental results and model predictions were due to possible errors associated with parameter determinations.

LDFM

Figures 8 and 9 present the sensitivity of the LDFM breakthrough predictions for the filter column with new sand and iron oxide coated sand for different values of the LDF rate constant k and the dispersion coefficient D_L. For both the media, iron breakthroughs were earlier when k was decreased or D_L was increased. The LDFM predictions for filter columns with coated sand, within the range of k and D_L tested, did not fit the experimental breakthrough values. This indicates that apart from mass transfer, some other mechanism may also be influencing the iron(II) adsorption capacity and, consequently, the shape of the iron breakthrough curve.

PFHSDM

Figures 10 and 11 present the effect of mass transfer coefficients (k_f, D_s) and adsorption capacity (K) on iron breakthrough curves for the filter columns with new sand and coated sand. Figure 10a shows that there was no significant change in the shape of the breakthrough curve with $\pm 50\%$ change in k_f, whereas some alteration of D_s and adsorption capacity K influenced both the shape of

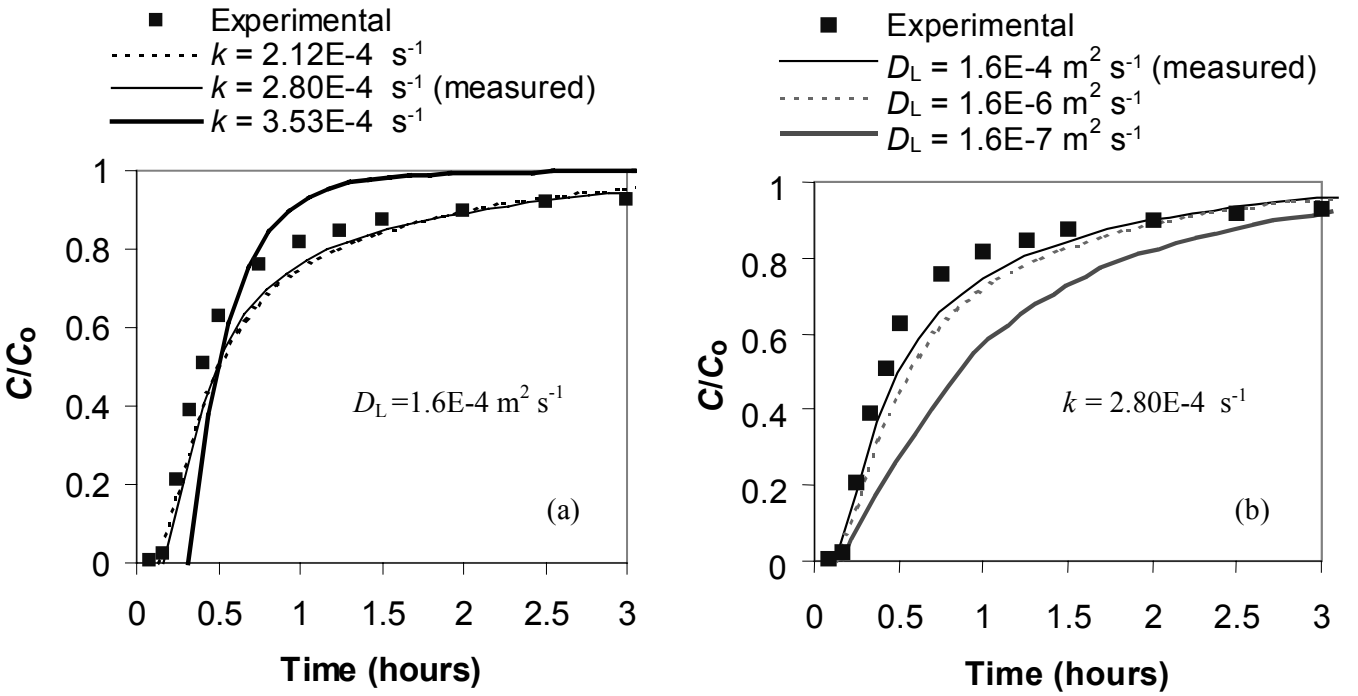

Figure 8 | Effect of (a) k and (b) D_L on the LDFM predictions of iron breakthrough for the filter column with new sand (pH=6.5, initial iron concentration=4 mg l^{-1}, filtration rate=8 m h^{-1}).

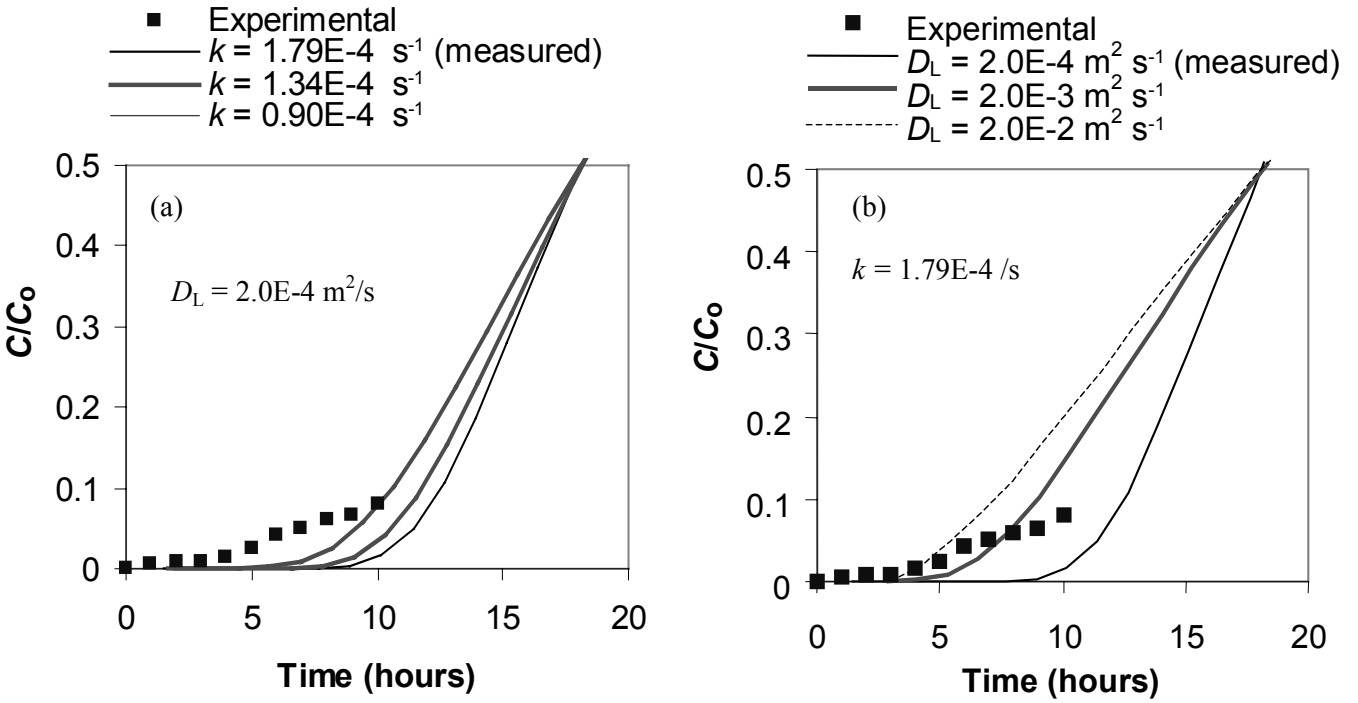

Figure 9 | Effect of (a) k and (b) D_L on the LDFM predictions of iron breakthrough for the filter column with iron oxide coated sand (pH=6.5, initial iron concentration=4 mg l^{-1}, filtration rate=4 m h^{-1}).

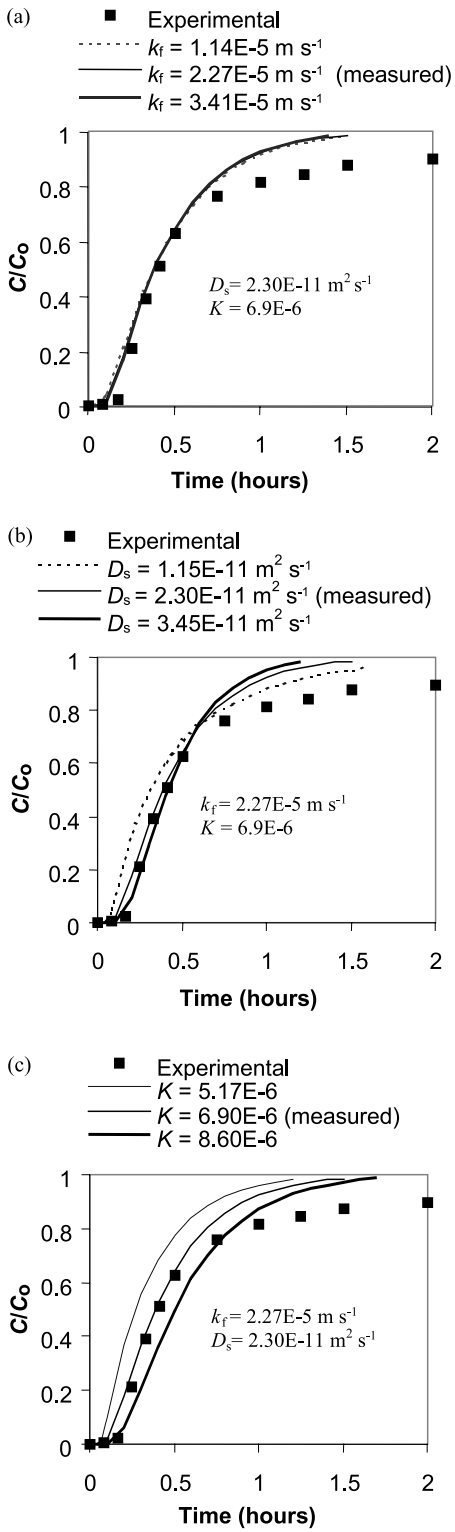

Figure 10 | Effect of (a) k_f, (b) D_s and (c) K on the PFHSDM predictions of iron breakthrough for the filter column with new sand (pH=6.5, initial iron concentration=4 mg l^{-1}, filtration rate=8 m h^{-1}).

the curve and breakthrough time significantly. In the case of iron oxide coated sand, a decrease in k_f and D_s influenced the initial part of the curve and gave early iron breakthrough (Figure 11). As expected, the breakthrough time was more sensitive to the changes in adsorption capacity K. However, in the case of coated sand, the breakthrough curve was very different from the model predictions with different sets of parametric value, indicating that the difference was not due to possible errors associated with the parameter determinations.

pH drop in the pores of filter media with iron(II) adsorption

In the case of filters with iron oxide coated sand, initial increases in filtrate iron concentrations were much earlier than those predicted by both the models (PFHSDM and LDFM). Further increases in iron concentrations were, however, much slower than the model predictions. It was hypothesised that the difference between the model predictions and the experimental results in this case was probably due to the 'pH drop' in the pores of the filter media due to iron(II) adsorption.

Adsorption of iron(II) onto filter media is accompanied by release of the proton (H^+) (Takai 1973; Barry *et al.* 1994), associated with a local pH drop in the pore spaces and on the surface of the filter media. This pH drop results in a temporary decrease in the iron(II) adsorption capacity. The extent of pH drop depends on the diameter of the pores and the density of adsorption sites. The BET nitrogen adsorption measurements showed that the coated sand tested had high pore volume (Table 1) and contained both micropores (diameter <2 nm) and mesopores (2 nm$<$diameter$<$50 nm). The calculated densities of iron(II) adsorption sites per unit BET specific surface area at equilibrium iron(II) concentration of 4 mg l^{-1} are presented in Table 6.

The proton released due to iron(II) adsorption, however, will react with the alkalinity (bicarbonate ions) present in water (e.g. diffusing from the bulk solution), thus compensating the pH change and regaining the iron(II) adsorption capacity.

$$H^+ + HCO_3^- \rightleftarrows CO_2 + H_2O \qquad (20)$$

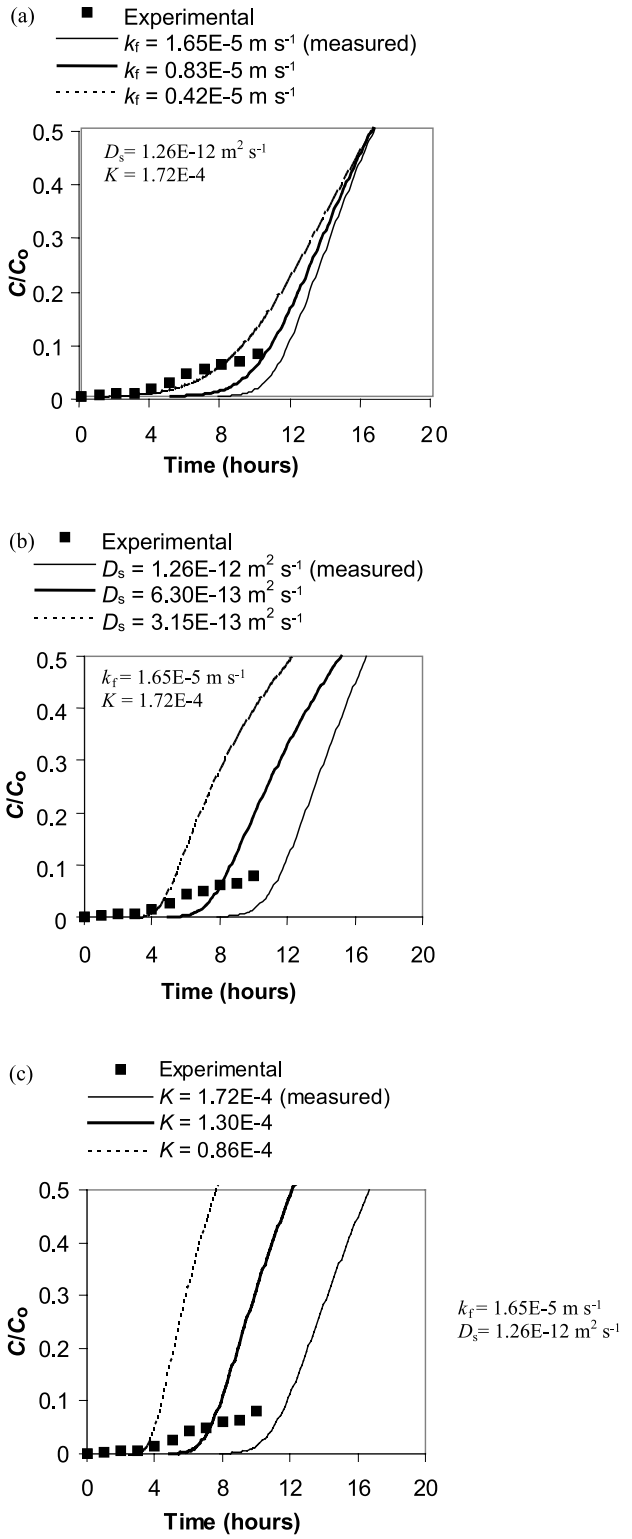

Figure 11 | Effect of (a) k_f, (b) D_s and (c) K on the PFHSDM predictions of iron breakthrough for the filter column with coated sand (pH=6.5, initial iron concentration=4 mg l^{-1}, filtration rate=4 m h^{-1}).

Table 6 | Density of iron(II) adsorption sites (iron(II) ions m^{-2})

	pH=6.0	pH=6.5	pH=7.0
New sand	1.91×10^{17}	2.04×10^{17}	3.17×10^{17}
Coated sand	2.40×10^{17}	3.44×10^{17}	6.60×10^{17}

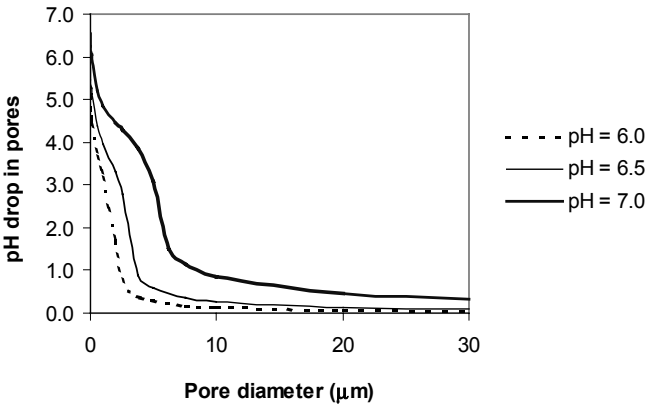

Figure 12 | pH drop in pores of iron oxide coated sand due to iron(II) adsorption at different pH as a function of pore diameter (HCO_3^-=100 mg l^{-1}, iron(II) concentration=4 mg l^{-1}).

Considering the filter media pore space as a closed system (no transport of H^+ and HCO_3^- out of the pore volume), the theoretical calculations of local pH drop in the pores of the filter media with iron(II) adsorption were made. Figure 12 shows that this local pH drop in the pores of the filter media with iron(II) adsorption is substantial for a pore diameter up to 5 μm, which consequently reduces the iron(II) adsorption capacity significantly.

The diffusion of H^+ ions outside the pores and/or transport of HCO_3^- ions inside the pores are time and concentration dependent processes governed by flow conditions, pore geometry and diffusion coefficients of H^+ and HCO_3^- ions. Therefore, it is likely that, initially, the iron breakthrough is faster than the model predictions as the adsorption capacity is lower (due to local pH drop). Later on, iron breakthrough is much slower as the adsorption capacity is much higher than before because of an increase of pH and also because the adsorption capacity, which was under-utilised initially, contributes to the overall adsorption.

This 'pH effect' on iron(II) adsorption is likely to be more pronounced at lower pH as the adsorption capacity decreases substantially with the decrease of pH. Additionally, this effect would be much less pronounced in the case of new sand as adsorption capacity is considerably smaller and, hence, the local pH drop with initial iron(II) adsorption is much lower. Furthermore, the pores in new sand are likely to be mainly close to the surface and relatively bigger than in iron oxide coated sand. Hence, the diffusion of H^+ and HCO_3^- is faster, and the pH drop would be minimal. In the case of coated sand, pore sizes are most likely much smaller and pores are much deeper inside the grain than those in new sand. Therefore, the pH effect is likely to be much more pronounced.

As mentioned earlier, in the short column tests, adsorption on the outer or external pore spaces is expected to be dominant, and this determines the mass transfer coefficients. The diffusion of iron(II) into the internal pores and subsequent pH drop due to iron(II) adsorption are also time-dependent. The internal pores are relatively much smaller than the external pores. The pH effect increases with a decrease in pore sizes. Therefore, it is likely that the 'pH effect' is less pronounced in the case of short column tests than in the long columns.

It should also be noted that in reality the actual pH drop is not so pronounced because, with the adsorption of iron(II), the pH starts to drop, consequently the adsorption capacity also decreases and all the adsorption sites available at the beginning are not occupied.

CONCLUSIONS

The process of adsorptive iron removal in filters under anoxic conditions was modelled using adsorption isotherm parameters, mass balance and mass transfer equations. The iron breakthroughs in adsorptive filters with new and iron oxide coated sand were predicted using three different models with increasing complexity, and the model predictions were compared with the experimental results. The following conclusions can be drawn:

- The experimental iron breakthrough in adsorptive filters occurred much earlier than the predictions of the constant pattern model (CPM), which considers film (external) mass transfer only. In addition, the shapes of the predicted iron breakthrough curves were considerably different from the experimental breakthrough curves.
- The linear driving force model (LDFM), which considers an overall mass transfer combining both external and internal mass transfer, gave a good prediction for the initial breakthrough in filter columns with new sand. However, the subsequent development gave a significant deviation. For coated sand, the model predictions improved but were still quite different from the measured values.
- The plug flow homogeneous surface diffusion model (PFHSDM), which separately includes both film mass transfer and surface diffusion, gave a good prediction of initial breakthrough in filter columns with new sand. Further development of the curve, as in the case of the LDFM, gave a significant deviation from experimental results. For coated sand, the iron breakthrough predictions with PFHSDM were not better than with the LDFM.
- Incorporating dispersion in the LDF and the PFHSDM gave no substantial improvement in iron breakthrough predictions.
- The difference in model predictions and experimental results in the case of iron oxide coated sand was probably due to the effect of an initial pH drop in the pores with iron(II) adsorption, and a consequent decrease in iron(II) adsorption capacity.
- More accurate predictions of iron breakthrough will require quantification of the effect of pH change in the pores of the filter media with iron(II) adsorption. In addition, the effect of inhomogeneity of pore sizes, and traces of oxygen in the water and in the pores needs to be studied in more detail.

ACKNOWLEDGEMENTS

This research was funded by Kiwa NV Water Research, Water Supply North West Brabant (WNWB), Water Supply Drenthe (WMD), Water Supply Gelderland (WG),

Water Supply Overijssel (WMO) and Water Supply East Brabant (WOB) in The Netherlands. Thanks are due to the laboratory staff of IHE for their help during the experimental work.

REFERENCES

Appelo, C. A. J., Drijver, B., Hekkenberg, R. & de Jonge, M. 1999 Modeling in situ iron removal from ground water. *Ground Wat.* **37**(6), 811–817.

Barry, R. C., Schnoor, J. L., Sulzberger, B., Sigg, L. & Stumm, W. 1994 Iron oxidation kinetics in an acidic alpine lake. *Wat. Res.* **28**(2), 323–333.

Bhattarai, R. R. & Griffin Jr, D. M. 1999 Results of tracer tests in rock-plant filters. *J. Environ. Engng-ASCE* **125**(2), 117–125.

Braester, C. & Martinell, R. 1988 The Vyredox and Nitredox methods of in situ treatment of groundwater. *Wat. Sci. Technol.* **20**(3), 149–163.

CRC Handbook of Chemistry and Physics (1996) 77th edition, CRC Press Inc., Boca Raton, USA.

Faust, S. D. & Aly, O. M. 1987 *Adsorption Processes for Water Treatment.* Butterworth Publishers, Boston, USA.

Hand, D. W., Crittenden, J. C. & Thacker, W. E. 1983 User-oriented batch reactor solutions to the homogeneous surface diffusion model. *J. Environ. Engng-ASCE* **109**(1), 82–101.

Hatva, T. 1989 *Iron and Manganese in Groundwater in Finland: Occurrence in Glacifluvial Aquifers and Removal by Biofiltration.* National Board of Waters and Environment, Helsinki, Finland.

Heijman, S. G. J., van Paassen, A. M., van der Meer, W. G. J. & Hopman, R. 1999 Adsorptive removal of natural organic matter during drinking water treatment. *Wat. Sci. Technol.* **40**(9), 183–190.

Levenspiel, O. 1972 *Chemical Reaction Engineering*, 2nd edition. John Wiley & Sons, Inc., New York, USA.

Liu, K. T. & Weber, W. J. Jr 1981 Characterization of mass transfer parameters for adsorber modeling and design. *J. Wat. Pollut. Cont. Fed.* **53**(10), 1541–1550.

Michaels, A. S. 1952 Simplified method of interpreting kinetic data in fixed bed ion exchange. *Ind. Engng Chem.* **44**(8), 1922–1930.

Mouchet, P. 1992 From conventional to biological removal of iron and manganese in France. *J. Am. Wat. Wks Assoc.* **84**(4), 158–167.

O'Connor, J. T. 1971 Iron & manganese. In: *Water Quality & Treatment–A Handbook of Public Water Supplies*. McGraw Hill, New York, pp. 378–396.

Peel, R. G. & Benedek, A. 1981 A simplified driving force model for activated carbon adsorption. *Can. J. Chem. Engng* **59**, December, 688–692.

Rott, U. 1985 Physical, chemical and biological aspects of the removal of iron and manganese underground. *Wat. Suppl.* **3**(2), 143–150.

Ruthven, D. M. 1984 *Principles of Adsorption and Adsorption Process.* John Wiley & Sons, New York, USA.

Salvato, J. A. 1992 *Environmental Engineering and Sanitation*, 4th edition. John Wiley & Sons, New York, USA.

Sharma, S. K., Greetham, M. & Schippers, J. C. 1999 Adsorption of iron(II) onto filter media. *J. Wat. Suppl.: Res. & Technol.-AQUA* **48(**3), 84–91.

Sharma, S. K., Kappelhof, J., Groenendijk, M. & Schippers, J. C. 2001 Comparison of physicochemical iron removal mechanisms in filters. *J. Wat. Suppl.: Res. & Technol.-AQUA* **50**(4), 187–198.

Sharma, S. K., Petrusevski, B. & Schippers, J. C. 2002 Characterisation of coated sand from iron removal plants. *Wat. Sci. & Technol.: Wat. Suppl.* **2**(2), 247–257.

Smith, E. H. 1991 Modified solution of homogeneous surface diffusion model for adsorption. *J. Environ. Engng-ASCE* **117**, 320–338.

Søgaard, E. G., Medenwaldt, R. and Abraham-Peskir, J. V. 2000 Conditions and rates of biotic and abiotic iron precipitation in selected Danish freshwater plants and microscopic analysis of precipitate morphology. *Wat. Res.* **34**(10), 2675–2682.

Sontheimer, H., Crittenden, J. C. & Summers, R. S. 1988 *Activated Carbon for Water Treatment.* AWWA-DVGW Forschungsstelle Engler Bunte Institut, Karlshue, Germany.

Standard Methods for the Examination of Water and Wastewater 1995 19th edition, American Public Health Association/American Water Works Association/Water Environment Federation, Washington, DC.

Takai, T. 1973 Studies on the mechanisms of catalytic deferrization (III)—Clarification of the mechanics of self catalytic deferrization. *J. Japan Wat. Wks Assoc.* **467**, August, 16–23.

Tamura, H., Goto, K. & Nagayama, M. 1976 The effect of ferric hydroxide on the oxygenation of ferrous ions in neutral solutions. *Corros. Sci.* **16**, 197–207.

Tien, C. 1994 *Adsorption Calculations and Modelling.* Butterworth-Heinemann, Boston, USA.

Wankat, P. C. 1990 *Rate Controlled Separations.* Elsevier Publishers Ltd., London, UK.

Weber, W. J., Jr 1972 *Physicochemical Processes for Water Quality Control.* John Wiley & Sons, Inc., New York, USA.

Weber, W. J. Jr & Liu, K. T. 1980 Determination of mass transport parameters for fixed bed adsorbers. *Chem. Engng Commun.* **6**, 264–270.

Wilson, E. J. & Geankoplis, C. J. 1966 Liquid mass transfer at very low Reynolds numbers in packed beds. *Ind. Engng Chem. Fund.* **5**(1), 9–14.

Yuasa, A. 1982 A Kinetic Study of Activated Carbon Adsorption Processes, PhD thesis, Hokkaido University, Sapparo, Japan.

First received 12 June 2002; accepted in revised form 30 May 2003